American Mineralogist, Volume 69, pages 1–15, 1984

High-pressure phase equilibria of a high-magnesia basalt and the genesis of primary oceanic basalts

DON ELTHON

Department of Geosciences
University of Houston, Houston, Texas 77004

AND CHRISTOPHER M. SCARFE

Experimental Petrology Laboratory
Department of Geology, University of Alberta
Edmonton, Alberta T6G2E3, Canada

Abstract

High-pressure phase equilibria studies on a high-MgO basalt from the Tortuga ophiolite complex indicate that olivine + orthopyroxene + clinopyroxene + garnet are its liquidus phases at 25 kbars. At 10 to 20 kbars, olivine is the liquidus phase and is followed by spinel, clinopyroxene, and orthopyroxene as temperature decreases. At <10 kbars, the order of crystalization is olivine, spinel, plagioclase, clinopyroxene, and orthopyroxene.

The high-pressure phase equilibria determined in this study, supplemented with the results obtained on other tholeiitic basalt compositions, are used to construct pseudo-liquidus phase diagrams for evaluating and predicting the nature of primary magmas and melting of the mantle at high pressures. These pseudo-liquidus phase diagrams suggest that "primitive" oceanic basalts with >9.5% MgO are derived from primary oceanic basalts generated at 15 to 25 kbars.

Models for the origin of oceanic basalts at low pressures (≤10 kbars) are considered incapable of generating the most "primitive" oceanic basalts that have >9.5% MgO. It is likely that most oceanic basalts with >9.5% MgO are ultimately derived from primary high-MgO basalts with >14% MgO that have been produced by melting at 15 to 25 kbars. High-MgO basalts of this type are found in numerous oceanic or rifting environments (*e.g.*, Baffin Bay, Gorgona Island, Tortuga ophiolite, Betts Cove ophiolite, Lewis Hills ophiolite, Ungava Peninsula), suggesting that these high-MgO basalts are produced on a world-wide scale throughout geologic time. Chemical differentiation processes, however, normally modify these high-MgO basalts into the more common basalts with 7 to 10% MgO. Because most oceanic basalts with <9.5% MgO have equilibrated to low-pressure cotectics, determination of the conditions of origin for the primary magmas from which they are derived is not well constrained. For this reason, melting of the mantle at pressures of ≤10 kbars could produce primary magmas capable of differentiating to form oceanic basalts that are similar to many of the evolved oceanic basalts that have <9.5% MgO. Until crystallization and mixing processes are more fully understood, melting at ≤10 kbars cannot be eliminated as a possibility for the origin of some primary oceanic basalts.

Introduction

Numerous models for the origin of oceanic basalts have been proposed and are being actively debated by petrologists and geochemists (e.g., O'Hara, 1968; Green *et al.*, 1979; Presnall *et al.*, 1979; Stolper, 1980; and references therein). One of the critical questions to be resolved in the controversy concerning the origin of oceanic basalts is the nature of primary magmas and their evolution within the crust and upper mantle. A broad consensus exists among petrologists and geochemists that oceanic basalts are ultimately derived by partial melting of the peridotitic sub-oceanic mantle. Primary magmas produced by melting under these conditions would have olivine (OL) + orthopyroxene (OPX)±clinopyroxene (CPX) and either garnet (GAR), spinel (SP), or plagioclase (PLAG) as liquidus phases at the pressure of final equilibration of the primary magma with the surrounding mantle. Especially critical in this regard is the requirement that primary basalts generated in the sub-oceanic mantle must be

0003–004X/84/0102–0001$02.00

multiply-saturated with OL + OPX because these two minerals are known to coexist with the liquid produced by partial melting of peridotites even at very large increments of fusion (Mysen and Kushiro, 1977; Jaques and Green, 1980; Scarfe *et al.*, 1979; Harrison, 1981, Elthon, 1981). As O'Hara (1968) originally proposed, most oceanic basalts do not have olivine as a liquidus phase at pressures $\geq$10 kbars and do not have orthopyroxene as a liquidus phase at any pressure. These factors, in conjunction with the observation that the Mg/(Mg + Fe) [the mg #] of most oceanic basalts is too low for them to have equilibrated with mantle olivines of $Fo_{>88}$ composition, indicate that most oceanic basalts are not primary magmas.

The main controversy, however, surrounding the nature of primary magmas that are generated in the suboceanic mantle is focused on the relatively "primitive" oceanic basalts that are characterized by high Ni contents (>200 ppm), high MgO contents (9.5 to 11% MgO), and generally low incompatible trace element abundances. These basalts are believed to have undergone the smallest extent of chemical differentiation prior to eruption, although the actual extent of this differentiation is contentious.

Previous studies of these "primitive" oceanic basalts by Green *et al.* (1979) and Bender *et al.* (1978) have shown that olivine disappears as a liquidus phase in "primitive" oceanic basalts at ~10 kbars and that orthopyroxene is not a liquidus phase in these basalts at any pressure that was experimentally investigated, as predicted by O'Hara. In fact, Green *et al.* (1979) demonstrated that DSDP basalt 3-18-7-1, one of the most "primitive" oceanic basalts recovered, was significantly displaced from the orthopyroxene primary phase volume at 12 kbars, requiring the addition of 9% orthopyroxene to the basalt before the basalt became saturated with orthopyroxene. Green *et al.* (1979) also demonstrated that DSDP basalt 3-18-7-1 required the addition of 17% olivine before co-saturation with both olivine and orthopyroxene was achieved at 20 kbars. On the other hand, Kushiro (1973) and Fujii and Kushiro (1977) present phase diagrams of two oceanic basalts that do show multiple saturation of OL + OPX + CPX + PLAG at the liquidus at 7.5 to 8 kbars. In the Kushiro (1973) and Fujii and Kushiro (1977) experiments, however, the liquidus orthopyroxenes in the experimental runs showing OL + OPX + CPX + PLAG saturation were too iron rich (mg# of 84 and 86, respectively) to have been in equilibrium with residual mantle OPX (mg# 88–91.5). In support of the proposal that some "primitive" oceanic basalts may be primary magmas, Fujii and Bougault (1983) have shown that OL + OPX + CPX + PLAG + SPINEL of an appropriate high-magnesium composition are on or near the liquidus of a "primitive" basalt from the FAMOUS area at 10 kbars.

One problem with many of these previous experimental studies is that the basalts chosen as the starting compositions have apparently undergone crystal fractionation prior to eruption. Attempts to deduce and then to adequately compensate for the pre-eruption history of these basalts introduced additional ambiguity into the interpretation of the origin of oceanic basalts.

In this study, we have chosen an aphyric high-MgO basalt (sample number NT-23) from the Tortuga ophiolite complex in southern Chile as our starting composition. This rock was selected because its high Mg/(Mg+Fe) [75.9] indicates equilibration with residual mantle olivines, the olivine microphenocrysts are appropriate for primary magmas (ave $Fo_{\sim 90.7}$), and its composition is similar to an estimated bulk composition of the oceanic crust (Elthon, 1979). Basalts from the Tortuga ophiolite complex (Elthon, 1980) are very similar to the FAMOUS basaltic glasses (Bryan and Moore, 1977) and other oceanic basalt suites (Melson *et al.*, 1977). High-MgO basalts broadly similar in composition to NT-23 have been reported from a number of localities (Baffin Bay: Clarke, 1970; Ungava Peninsula: Francis and Hynes, 1979; Betts Cove ophiolite: Upadhyay 1978; Gorgona Island: Echeverria, 1980; Lewis Hills Massif of the Bay of Islands ophiolite: Karson *et al.*, 1983) suggesting that these high-MgO basalts are produced on a world-wide scale throughout geological time, and that chemical differentiation processes normally modify these high-MgO basalts into the more abundant basalts with 7 to 10% MgO.

This experimental study shows that a high-MgO basaltic liquid, similar in composition to NT-23, is multiply saturated with olivine + orthopyroxene + clinopyroxene + garnet at 25 kbars. The preliminary results of this study have been previously described by Elthon and Scarfe (1980).

Experimental procedure

Chips of the fine-grained margin of the rock (Table 1) were powdered in a tungsten–carbide vial of a Spexmill. The powder was further ground under acetone for 3 hours, then dried for 20 hrs. at ~1100°C at the QFM oxygen fugacity buffer to decompose secondary alteration products. The powder was stored in a drying oven at ~110°C between runs.

The powder was loaded into graphite containers, heated until red, and then sealed inside 3mm O.D. platinum capsules. A pyrex glass sleeve around the heating element inhibited water access to the sample region and minimized hydrogen diffusion into the capsule. The internal graphite capsules prevented iron loss from the sample to the platinum capsule and maintained a relatively low fo_2 at the graphite-CO buffer. Because graphite capsules were used in these experiments, a minor amount of CO may have dissolved in the melt at high pressures (*e.g.*, Green *et al.*, 1979). The amount of CO in the melt is presumed to be small because the electron microprobe analyses of the glasses sum to near 100% (see Table 3).

All experiments were conducted with a solid-media, high-pressure apparatus with a ½ in. diameter furnace

Table 1. Major element composition of NT-23

	Bulk Rock[a]	Fine-Grained Margin[b]
SiO_2	47.25	47.73 ± .27
TiO_2	.79	.85 ± .03
Al_2O_3	13.64	13.42 ± .23
FeO	9.77	9.58 ± .24
MgO	17.61	16.89 ± .18
CaO	9.58	9.94 ± .14
K_2O	.06	0.05 ± .02
Na_2O	.89	1.07 ± .03
MnO	.14	.20 ± .03
Total	99.73	99.73

[a]From Elthon (1979)

[b]Average of glass compositions from runs 304, 306, 313, 320, 328.

assembly (Boyd and England, 1960). The piston-out technique was used with a −4% correction for friction. The quoted pressures given in Table 1 are considered accurate to ±1 kbar. Temperatures were monitored with Pt_{100}-$Pt_{90}Rh_{10}$ thermocouples and were automatically controlled (Hadidiacos, 1972) with an accuracy of ±10°C. Most runs were 1 hour in duration. The observation that no change occurred in the phase equilibria between experiments of 1 and 10 hrs. duration of 25 kbars and 1470° was taken to indicate that equilibrium was achieved in the shorter runs.

All phase identifications have been verified with the electron microprobe. The microprobe analyses reported here were determined on an ARL-SEMQ nine-channel microprobe housed at the Department of Mineral Sciences at the Smithsonian Institution using the standard analytical techniques described by Melson (1978). Standards of natural basaltic glasses were used for glass analyses, natural olivines for the olivine analyses, and natural pyroxenes and amphiboles for the pyroxene analyses. All of the samples are corrected for matrix effects by the method of Bence and Albee (1968) and Albee and Ray (1970). Clinopyroxene crystals in the experimental charges are often small and are difficult to analyze with high-quality because of overlap with the surrounding glass. Unless otherwise noted below for a specific run, this problem was not significant for other minerals.

Results

The high-pressure phase equilibria of high-MgO basalt NT-23 are shown in Figure 1. The pressure, temperature, duration, and run products of the experiments are listed in Table 2. Olivine (±spinel) is the liquidus phase at pressures of <25 kbar, but the temperature interval for olivine-only (±spinel) crystallization diminishes with increasing pressure from ≪150°C at 10 kbars to <10° at 25 kbar. The sequence in which minerals crystallize in NT-23 changes from OL–SP–PLAG–CPX at 1 atm to OL–SP–CPX–OPX at 10–20 kbars. At 25 kbar and 1470°C, olivine, orthopyroxene, clinopyroxene, and garnet are co-liquidus phases. This is the only pressure at which a lherzolite assemblage is on the liquidus of NT-23. The results of 1 atmosphere runs, which were done on 0.003 in. diameter Pt wire loops at the QFM oxygen fugacity buffer, will be reported elsewhere with the 1 atm experimental phase relationships of other basalts from Tortuga.

10 kbar

Olivine is the liquidus phase at 10 kbars and crystallizes alone (±a trace of spinel) for ~150°C; clinopyroxene begins to crystallize with olivine + spinel at 1230°;

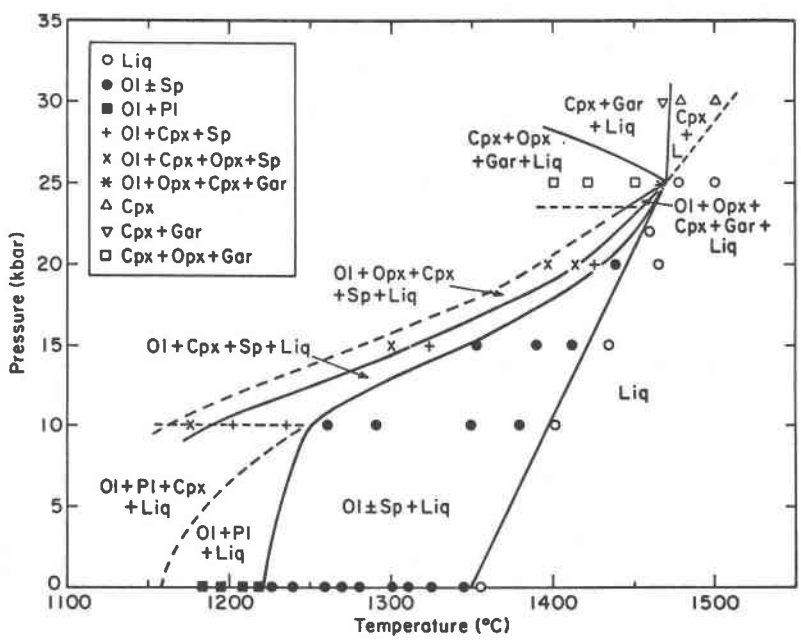

Fig. 1. Phase diagram for NT-23.

Table 2. Summary of experimental results

Pressure (Kbars)	Temperature (°C)	Run Number	Time (hrs.)	Phases Present
10	1400	313	1	GL
10	1390	308	1	GL + OL
10	1380	317	1	GL + OL
10	1350	315	1	GL + OL
10	1320	316	1	GL + OL + SP
10	1290	324	1	GL + OL
10	1260	323	1	GL + OL + SP
10	1230	329	1	GL + OL + SP + CPX
10	1200	331	1	GL + OL + CPX
10	1170	333	1	GL + OL + SP + CPX + OPX + PLAG
15	1435	320	1	GL
15	1410	319	1	GL + OL
15	1390	318	1	GL + OL + SP
15	1350	325	1	GL + OL
15	1325	326	1	GL + OL + SP + CPX
15	1300	330	1	GL + OL + SP + CPX + OPX
20	1465	306	1	GL
20	1440	307	1	GL + OL
20	1425	163	1	GL + OL + SP + CPX
20	1420	310	1	GL + OL + SP + CPX + OPX + Quench Pyroxenes
20	1420	310A	1	GL + OL + SP + CPX + OPX
20	1400	309	1	GL + OL + SP + CPX + OPX
22.5	1460	321	1	GL
25	1475	304	1	GL
25	1470	328	1	GL
25	1470	164	10	GL + OL + CPX + OPX + GAR
25	1465	332	1	GL + OL + CPX + OPX + GAR
25	1463	314	1	GL + CPX + OPX + GAR
25	1450	302	1	CPX + OPX + GAR + Quench Pyroxenes
25	1425	305	1	CPX + OPX + GAR + Quench Pyroxenes
25	1400	303	1	CPX + OPX + GAR + Quench Pyroxenes
30	1500	322	1	CPX + Quench Pyroxenes
30	1485	311	1	CPX + Quench Pyroxenes
30	1465	312	1	CPX + GAR + Quench Pyroxenes + Cu, Ni, Fe Sulphide

orthopyroxene, and plagioclase crystallize with olivine, clinopyroxene and spinel at 1170°C. Using a least squares mixing program (Bryan *et al.*, 1969), we have calculated the weight percentages of the various phases in each of the experimental runs. The results of these calculations are given at the bottom of Table 3. Spinel was not included as a mineral in these mass balance calculations because spinel occurs in only trace amounts of very small crystals that are generally too small to quantitatively analyze with the electron microprobe.

Olivine (±spinel) crystallizes alone until ~18% olivine crystals have formed. The composition of the first olivine to crystallize in the 10 kbar experimental runs is $Fo_{90.5}$ but, by extrapolation of results from lower temperatures, it is likely that the liquidus olivine is $Fo_{90.8-91.0}$. The olivines become more iron-rich during crystallization as the liquid becomes depleted in MgO and enriched in those elements that are incompatible in olivine. Notice that the glass compositions are basaltic in character along the isobaric OL + CPX + SP + LIQ pseudo-univariant curve and at the OL + OPX + CPX + SP + PLAG + LIQ pseudo-invariant point.

15 kbar

Olivine ± spinel is the liquidus phase at 15 kbars. CPX begins to crystallize at ~1325°(~100° below the liquidus) and OPX begins to crystallize at ~1300°. Olivine crystallizes alone (±spinel) for the first 12%, OL + CPX + SP over the interval from 12–15% crystallization, and OL + OPX + CPX + SP from 15–17% crystallization.

20 kbar

Olivine is the liquidus phase but its crystallization interval is much smaller (~30°C; ~6% crystals) than at lower pressures. The isobaric pseudo-invariant point is reached after only 8% crystallization.

25 kbar

Olivine, orthopyroxene, clinopyroxene and garnet coexist with a high-MgO basaltic liquid on the liquidus or within 10° of it at 25 kbars. Only a trace amount of crystals (<2%) was formed in run 164 at 1470°C. The olivine ($Fo_{89.5}$) and the orthopyroxene (mg = 90.4) formed crystals that were large enough to easily analyze with the microprobe. The clinopyroxene and garnet crystals were very small and it is possible that those analyses include overlap with some of the adjacent glass. At temperatures below 1465°, olivine has not been observed as a run product. This absence is in agreement with the OL + LIQ ⇄ GAR + OPX + CPX reaction of Kushiro and Yoder (1974).

30 kbar

The phase relationships have been determined on a reconaissance basis at 30 kbars. CPX is the liquidus phase at 30 kbars and garnet is the second mineral to crystallize. The extensive development of quench pyroxene overgrowths precluded meaningful analysis of the run products at 30 kbars.

Discussion of results

Spatial location of isobaric pseudo-invariant points in natural basalt–mantle systems

Coexistence of four mineral phases with a silicate liquid at a specified pressure defines an isobaric invariant point in a quaternary system. Presnall *et al.* (1979) have determined the chemical compositions of silicate liquids coexisting with olivine, orthopyroxene, clinopyroxene, and either plagioclase (at <9.3 kbar) or spinel (at ≥9.3 kbar) for 6 isobaric invariant points at 1 atm to 20 kbar pressure in the quaternary $CaO–MgO–Al_2O_3–SiO_2$ system. Hoover and Presnall (1981) have extended this earlier work into the sodium-bearing synthetic system at 1 atm to 20 kbar.

Stolper (1980) attempted to equilibrate basaltic glass from the project FAMOUS area of the Mid-Atlantic Ridge with an olivine + orthopyroxene ± clinopyroxene assemblage at 10, 15, and 20 kbar pressure in order to constrain the compositions of liquids saturated with these minerals (OL + OPX ± CPX) in the natural multicomponent basalt-mantle system. The glass compositions reported by Stolper (1980) were not in equilibrium with spinel and, therefore, they represent compositional points along the

OL + OPX + CPX + LIQ isobaric pseudo-univariant curves or the OL + OPX + LIQ isobaric pseudo-divariant surface. It is uncertain, however, whether this absence of spinel saturation is of much significance, because of the low abundance of spinel in the upper mantle and its complex solid solution behavior.

In an effort to evaluate the compositions of liquids at isobaric pseudoinvariant points in the natural basalt–mantle system, we use the compositions of glasses from runs 164 (25 kbar), 310A and 309 (20 kbar), 330 (15 kbar), and 333 (10 kbar) as well as the results of high-pressure experiments on other tholeiitic basalt compositions. These high-pressure phase equilibria are projected from clinopyroxene onto the olivine–plagioclase–silica plane (Fig. 2) and from anorthite onto the olivine-clinopyroxene-silica plane (Fig. 3). For details of the projection method, see Elthon (1983).

Several of the compositions studied show multiple-saturation involving olivine + orthopyroxene±other phases at high pressures. In addition to the isobaric pseudo-invariant points derived from NT-23 (runs 164, 309, 330, and 333) and Fujii and Bongault (1983), the olivine basalt (O.B.) studied by Green and Ringwood (1967) crystallized olivine + orthopyroxene + clinopyroxene just below the liquidus at 9 kbar. The oceanic tholeiite (395A) studied by Fujii and Kushiro (1977) has olivine + orthopypoxene + clinopyroxene + plagioclase just below the liquidus at 7.5 kbar. Kushiro (1973) found that olivine tholeiite T-87 has olivine + orthopyroxene + clinopyroxene + plagioclase as liquidus phases at 8 kbar. Basalt 66018 from Skye (Thompson, 1974) has olivine as the liquidus phase at <16.5 kbars and clinopyroxene at higher pressures. Slightly below the liquidus in the pressure interval of ~14 to 16 kbar, olivine + orthopyroxene + clinopyroxene ± spinel(?) are in equilibrium with the liquid, indicating that the composition of this basalt lies close to the 15 kbar pseudo-invariant point.

The olivine tholeiite (O.T.) of Green and Ringwood (1967) has olivine as a liquidus phase up to 13.6 kbar. At pressures ≥13.6 kbars and <22.5 kbar, orthopyroxene is the liquidus phase with clinopyroxene as the second phase. At pressures of ≥22.5 kbar, clinopyroxene is the liquidus phase. These experiments agree with the shift in phase equilibrium boundaries at high pressures as shown in Figures 2 and 3.

The picrite of Green and Ringwood (1967) has olivine + clinopyroxene + garnet within 20° of the liquidus at 22.5 kbar and orthopyroxene + clinopyroxene + garnet just below the liquidus at 27.5 kbar. These experiments suggest that at ~25 kbar olivine + orthopyroxene + clinopyroxene + garnet would be on or near the liquidus for this composition.

The 1840 picrite of Tilley and Yoder (1964) has olivine as the liquidus phase, orthopyroxene is second, clinopyroxene is third and garnet is the fourth phase to crystallize at 20 kbar. These phase equilibria also agree with the shift in boundaries as shown in Figure 2 and 3.

The phase equilibria boundaries as shown in Figures 2 and 3 are also supported by the high-pressure experimental results obtained on two of the most "primitive" oceanic basalts. Green *et al.* (1979) found that olivine is the liquidius phase of DSDP basalt 3-18-7-1 up to 10 kbar and that olivine is replaced by clinopyroxene as the liquidus phase at higher pressures. Orthopyroxene was not observed within the *P–T* interval studied and even with the addition of 5% orthopyroxene to the sample, the liquid did not become saturated with orthopyroxene at 12 kbar. It took the addition of 9% orthopyroxene to the starting basalt in order to saturate the resulting liquid with orthopyroxene. Green *et al.* added 9% olivine to the starting basalt and found that at 15 kbar, this mixture had olivine + clinopyroxene as the liquidus phases and that at higher pressures, clinopyroxene was the liquidus phase. Orthopyroxene was not found in any of these experiments. By mixing 17% olivine with the starting basalt, Green *et al.* found that olivine was the liquidus phase at 20 kbar, but that olivine + orthopyroxene were near liquidus phases.

Bender *et al.* (1978) determined the phase relationships for project FAMOUS basalt 527-1-1 at 0 to 15 kbar. Their data indicate that olivine is the liquidus phase at pressures ≤11 kbars and clinopyroxene is the liquidus phase at higher pressures. Even though Bender *et al.* state that 527-1-1 "is multiply saturated at 10.5 kbar with olivine, clinopyroxene, and orthopyroxene", orthopyroxene is not observed as a liquidus phase at any pressure. The 15 kbar results of Bender *et al.* show that clinopyroxene is the liquidus phase but is replaced by orthopyroxene at lower temperatures. This elimination of clinopyroxene and its replacement by orthopyroxene requires a CPX + LIQ ⇄ OPX reaction relationship. This reaction does not occur unless a plane tangential to the OPX + CPX + LIQ surface intersects the *extension* of the OPX_{ss}–CPX_{ss} join at the orthopyroxene end. This tangential plane lies close to natural clinopyroxene compositions and it is possible that a reaction eliminating orthopyroxene but not clinopyroxene will occur. In an effort to evaluate the proximity of basalt 527-1-1 to the orthopyroxene primary phase volume, Bender (pers. comm., 1981) has tried orthopyroxene addition experiments similar to those of Green *et al.* (1979) and found that the 527-1-1 liquid at 15 kbar and 1310° is not in equilibrium with orthopyroxene. Presumably, the orthopyroxene at 15 kbar reported by Bender *et al.* (1978) was a metastable product.

These results from several different laboratories form a reasonably consistent data set for the locations of upper mantle phase equilibria boundaries. This arrangement of phase equilibria boundaries (Figs. 2 and 3) is not very consistent with the melting relationships of natural peridotites. The results from partial melting of peridotites (not shown) scatter incoherently across these diagrams, a feature that we believe is a consequence of the difficulty in determining the equilibrium composition of the small

Table 3. Electron microprobe analyses of run products

10 Kbar Run Products

Run Number Phase	313 Glass	308 Glass	308 Olivine	317 Glass	317 Olivine	315 Glass	315 Olivine	316 Glass	316 Olivine
SiO_2	47.31	47.82	41.00	47.96	40.78	49.14	40.63	49.21	40.01
TiO_2	.83	.85	-	.89	-	.92	-	1.04	-
Al_2O_3	13.37	13.84	.00	14.21	.04	15.20	.04	16.04	.14
Cr_2O_3	-	-	.15	-	.18	-	.19	-	.17
FeO	9.62	9.66	9.28	9.68	9.44	9.74	10.59	9.45	11.24
MgO	16.71	15.94	49.45	15.02	49.07	12.85	47.39	11.65	46.68
MnO	-	.16	.13	.15	.16	.15	.13	-	.15
NiO	-	-	.24	-	.22	-	.23	-	-
CaO	10.03	10.40	.31	10.59	.37	11.37	.41	11.70	.39
Na_2O	1.08	1.10	-	1.15	-	1.16	-	1.17	-
P_2O_5	.09	-	-	.06	-	.11	-	.10	-
K_2O	.08	.05	.07	.05	.02	.05	.01	.40	.02
Sum	99.13	99.82	100.63	99.76	100.28	100.69	99.62	100.40	98.80
100 × Mg/(Mg+Fe)	75.6	74.6	90.5	73.4	90.3	70.2	88.9	68.7	88.1
Wt % of Phase	100%	97%	3%	94%	6%	87%	12%	85%	15%

Run Number Phase	323 Glass	323 Olivine	329 Glass	329 Olivine	329 CPX	331 Glass	331 Olivine	331 CPX	333 Glass	333 Olivine	333 CPX
SiO_2	48.41	40.48	48.81	40.75	49.11	48.86	40.16	49.32	48.99	39.63	49.28
TiO_2	1.07	-	1.18	-	.74	1.18	-	.89	1.41	-	1.08
Al_2O_3	16.27	.07	16.84	.10	5.11	17.20	.13	5.87	17.92	.20	5.66
Cr_2O_3	-	.16	.15	.13	.20	-	.14	-	-	.17	.27
FeO	9.22	10.68	9.07	11.68	7.77	9.43	12.56	8.17	10.01	15.98	7.45
MgO	9.91	47.83	9.47	46.90	16.40	8.92	46.13	15.44	8.62	42.69	15.33
MnO	-	.15	.13	.11	.17	.18	.20	.20	.20	.23	.21
NiO	-	.23	-	-	-	-	-	-	-	.20	-
CaO	12.30	.38	12.20	.39	19.24	11.72	.37	19.77	11.21	.70	21.04
Na_2O	1.31	-	1.42	-	.29	1.71	-	.31	2.02	-	.31
P_2O_5	.07	-	-	-	-	-	-	-	-	-	-
K_2O	.06	.02	.01	.00	-	.05	.01	-	.06	.03	-
Sum	98.62	100.00	99.28	99.96	99.03	99.25	99.70	99.97	100.44	99.83	100.63
Mg-number	65.7	88.9	65.0	87.7	79.0	62.8	86.7	77.1	60.6	82.6	78.6
Wt % of Phase	82%	18%	80%	20%	1%	75%	20%	5%	32%	10%	18%

pockets of glass that are produced during melting of peridotites.

Melting of the sub-oceanic mantle

These high-pressure phase diagrams can be used for evaluating melting in the mantle and the production of primary oceanic basalts. We emphasize that these are limitations to the application of these pseudo-liquidus phase diagrams. For example, all of the phase relations here are for anhydrous systems and are strictly applicable only to melt production in an anhydrous environment. For oceanic basalts, this is probably not a major concern because of the low water contents of oceanic basalts (Moore, 1970; Delaney *et al.*, 1978). For very small increments of melting of natural peridotites, where accessory phases such as phlogopite, apatite, amphibole, or carbonate may be present and the influence of CO_2 and H_2O may be important, it is likely that these phase diagrams do not adequately portray the true variations in liquid compositions. Finally, it should be noted that there

Table 3. (cont.)

15 Kbar Run Products

Run Number	320	319	319	318	318	325	325	326	326	326	330	330	330	330
Phase	Glass	Glass	Olivine	Glass	Olivine	Glass	Olivine	Glass	Olivine	CPX	Glass	Olivine	CPX	OPX
SiO_2	47.93	47.81	40.99	48.31	40.10	48.57	39.82	48.65	39.87	52.90	48.55	40.14	53.03	54.01
TiO_2	.85	.95	-	.92	-	.95	-	.95	-	.51	1.19	.20	.62	.22
Al_2O_3	13.79	14.72	.09	15.06	.09	15.56	.10	15.86	.09	4.71	15.95	.11	4.93	3.79
Cr_2O_3	-	-	.09	-	.16	-	.12	-	.09	.16	.07	.08	.10	.40
FeO	9.98	9.97	8.47	9.78	9.16	9.77	9.47	9.57	10.56	6.87	9.48	13.48	7.32	11.79
MgO	16.88	13.92	49.20	13.50	49.00	12.59	48.93	12.19	48.65	19.78	11.99	46.22	18.19	27.79
MnO	-	-	.13	-	.15	-	.15	.16	.17	.22	.11	.16	.19	.21
NiO	-	-	.44	-	.42	-	.40	-	.39	-	-	-	-	-
CaO	9.95	10.92	.31	11.08	.34	11.29	.34	11.65	.31	15.69	11.76	.29	15.91	2.14
Na_2O	1.12	1.23	-	1.17	-	1.23	-	1.18	-	.20	1.31	.00	.20	.06
P_2O_5	.09	.10	-	.06	-	.11	-	-	-	-	-	-	-	-
K_2O	.04	.05	.00	.03	.05	.07	.01	.05	.01	-	.02	.00	-	-
Sum	100.62	99.67	99.72	99.91	99.47	100.14	99.34	100.26	100.14	101.04	100.43	100.68	100.49	100.41
Mg-number	75.1	71.3	91.2	71.1	90.5	69.7	90.2	69.4	89.1	83.7	69.3	85.9	81.6	80.8
Wt % of Phase	100%	92%	8%	90%	10%	88%	12%	85%	13%	2%	83%	12%	2%	3%

20 Kbar Run Products

Run Number	306	307	307	310A	310A	310A	310A	309	309	309	309
Phase	Glass	Glass	Olivine	Glass	Olivine	CPX	OPX	Glass	Olivine	CPX	OPX
SiO_2	47.65	47.82	39.98	48.02	39.53	50.54	54.53	48.11	40.05	49.85	53.25
TiO_2	.81	.88	-	.92	-	.86	.29	.97	.10	.75	.20
AL_2O_3	13.42	14.31	.16	14.48	.12	6.88	4.61	14.65	.15	7.69	4.86
Cr_2O_3	-	-	.16	.11	.14	.18	.25	.21	-	.29	.28
FeO	9.51	9.65	10.20	9.35	11.20	7.12	8.12	9.40	11.69	7.28	8.65
MgO	17.09	14.85	47.99	14.67	47.54	18.06	28.26	14.50	47.09	18.71	28.86
MnO	.22	-	.12	.13	.15	.20	.18	.16	.17	.20	.19
Nio	-	-	.37	-	.45	-	-	-	-	-	-
CaO	9.71	10.67	.36	10.98	.33	15.07	3.10	11.08	.30	15.16	3.44
Na_2O	1.06	1.23	-	1.32	-	.22	.08	1.27	.00	.27	-
P_2O_5	-	.10	-	-	-	-	-	-	-	-	-
K_2O	.05	.04	.02	.01	.02	.00	.01	.03	.00	.00	.00
Sum	99.52	99.55	99.36	99.99	99.48	99.13	99.43	100.38	99.55	100.20	99.82
Mg-number	76.2	73.3	89.3	73.7	88.3	81.9	86.1	73.3	87.8	82.1	86.6
Wt % of Phase	100%	94%	6%	92%	5%	trace	4%	90%	5%	trace	5%

is a finite, but poorly defined, width of the phase equilibrium boundaries in the diagrams as a consequence of analytical uncertainty and variations in the composition of the basalts (such as Fe/Mg) that are not compensated for in the formulation of the end member minerals.

From these pseudo-liquidus phase diagrams it is possible to obtain information on the nature of primary melts and the effects of crystallization at high and low pressures. Information on the types of residual ultramafic rocks in equilibrium with primary magmas can also be obtained from pseudo-liquidus phase diagrams. In this manner, melts projecting at the isobaric pseudo-invariant points would be in equilibrium with an aluminous (garnet/spinel/plagioclase) lherzolite whereas liquids projecting along an OL + OPX + SP + LIQ isobaric pseudo-univariant curve would be in equilibrium with a spinel harzburgite residuum. In principle, the study of these residual ultramafic rocks will provide critical information on the nature of primary magmas.

Information on residual ultramafic mantle rocks related to oceanic basalt petrogenesis is obtained from ophiolites and oceanic fracture zones. Bonatti and Hamlyn (1981) conclude, in a survey of oceanic ultramafic rocks, that harzburgite is slightly more common than lherzolite in the rift zones of the Indian Ocean Ridge (Dmitriev, 1969) and within fracture zones of the equatorial Atlantic Ocean (Bonatti *et al.*, 1970; Melson and Thompson, 1971). In some of the major fracture zones of the western Indian

Table 3. (cont.)

25 Kbar Run Products							
Run Number Phase	304 Glass	328 Glass	164 Glass	164 Olivine	164 CPX	164 OPX	164 GARNET
SiO_2	48.02	47.72	47.85	40.21	50.24	53.29	41.21
TiO_2	.89	.86	.90	-	.62	.15	2.08
Al_2O_3	13.16	13.38	13.82	.07	7.39	6.64	17.67
Cr_2O_3	.20	-	-	.12	.21	-	.79
FeO	9.41	9.37	9.86	10.10	5.81	6.43	9.27
MgO	17.06	16.72	16.61	48.31	18.31	30.53	17.10
MnO	.21	.17	.17	.17	.14	.11	.22
NiO	-	-	-	-	-	-	-
CaO	9.94	10.06	10.87	.32	16.01	2.43	8.72
Na_2O	1.04	1.07	.95	.00	.21	.12	.73
P_2O_5	-	-	-	-	-	-	-
K_2O	.01	.06	.06	.01	.00	.02	.02
Sum	99.94	99.41	101.09	99.24	98.94	99.72	97.81
Mg-number	76.4	76.1	75.0	89.5	84.9	89.4	76.7

Ocean (Engel and Fisher, 1975; Bonatti and Hamlyn, 1978; Hamlyn and Bonatti, 1980) lherzolites are more common than harzburgites. In the major ophiolite bodies, residual mantle harzburgite is much more abundant than lherzolite (Samail: Boudier and Coleman, 1981; Bay of Islands: Casey *et al.*, 1981; Papua-New Guinea: Davies, 1971; Troodos: Wilson 1959; Vourinos: Jackson *et al.*, 1975) although residual mantle lherzolites are reported from some alpine ophiolites.

Although published mineral chemistry data on oceanic or ophiolitic residual mantle rocks are limited, these data indicate that there are only minor differences in the mineral compositions in orthopyroxenes and olivines from harzburgites and lherzolites (Hamlyn and Bonatti, 1980; H. Dick, pers. comm.). During progressive melting of mantle assemblages, the Mg/(Mg+Fe) of residual minerals should gradually increase (*e.g.*, Jaques and Green, 1980). Because of the similarity of olivine and orthopyroxene compositions in harzburgites and lherzolites, it is likely that many of the harzburgites are the residuum of a partial melting event in which the degree of melting progressed just slightly beyond the disappearance of the final residual clinopyroxene crystals.

The above data on residual mantle rocks from ophiolites and oceanic fracture zones would suggest that a range of melting conditions probably occurs within the suboceanic mantle, in some cases leaving a lherzolite residuum and in other instances, a harzburgite residuum. For the genesis of oceanic basalts, a continuum of models ranging from a lherzolite to a harzburgite residuum should be considered.

Pressure of origin for primary oceanic basalts

O'Hara (1968) and Walker *et al.* (1979) have shown that most oceanic basalts cluster near the 1 atm olivine + plagioclase + clinopyroxene + liquid pseudo-univariant curve and presumably have been affected by low-pressure crystal fractionation. As noted above, however, the main controversy in the origin of primary oceanic basalts concerns those rare relatively "primitive" basalts with >9.5% MgO, which are interpreted to have undergone the least amount of differentiation prior to eruption.

In the discussion that follows it is assumed that the majority of oceanic basalts, those with <9.5% MgO, are ultimately derived by crystallization and magma mixing processes from parental liquids whose major element compositions are very similar to these "primitive" oceanic basalts shown in Figures 2 and 3. This type of assumption, that the basaltic liquids with the highest MgO contents (or Mg number) are parental to the more evolved basaltic liquids with lower MgO contents (or Mg number), is very commonly made in modeling crystal fractionation and other evolutionary processes in oceanic basalt petrogenesis. Because we believe that this assumption is valid in most suites of oceanic basalts, we initially discuss our data within this context. In the final section, we note that this assumption may not always be valid, but that some oceanic basalts might be derived from "primitive" magmas that are distinctly different from those with >9.5% MgO that are shown in Figures 2 and 3.

Figure 4, which is a plot of the MgO content of basaltic glasses versus the amount of normative silica (data from

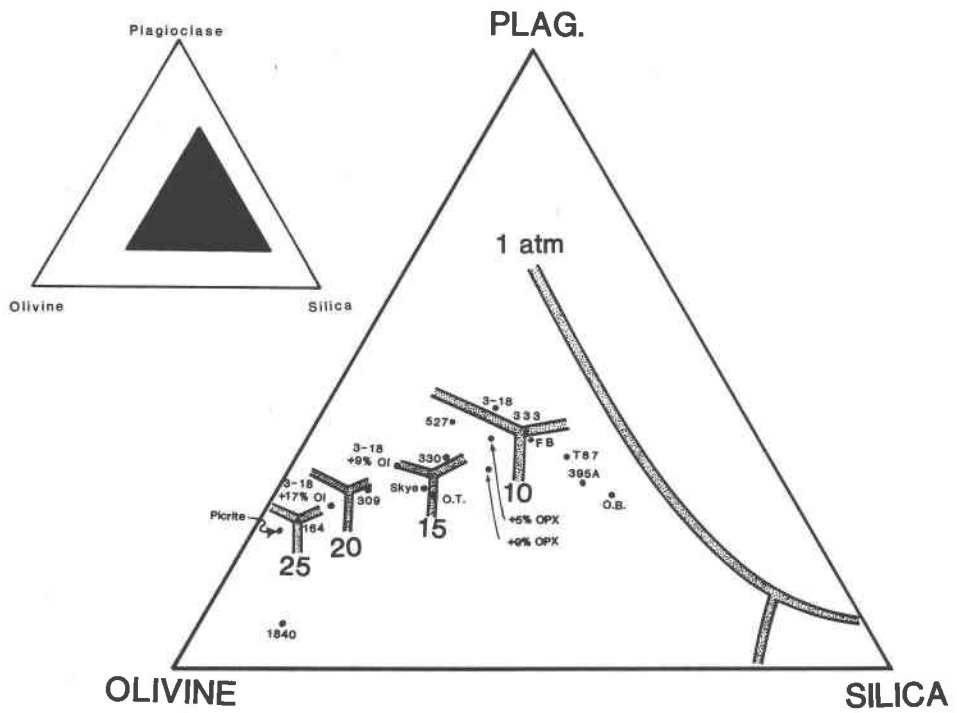

Fig. 2. Pseudo-liquidus phase diagram projected from clinopyroxene. See text for discussion. The apices of the triangle are: (top) $AN_{65}OL_{10}SIL_{25}$ (left) $OL_{60}AN_{15}SIL_{25}$ (right) $SIL_{75}AN_{15}OL_{10}$. Details of the projection method are given in Elthon (1983). 1 atm phase equilibria are from Walker *et al.* (1979).

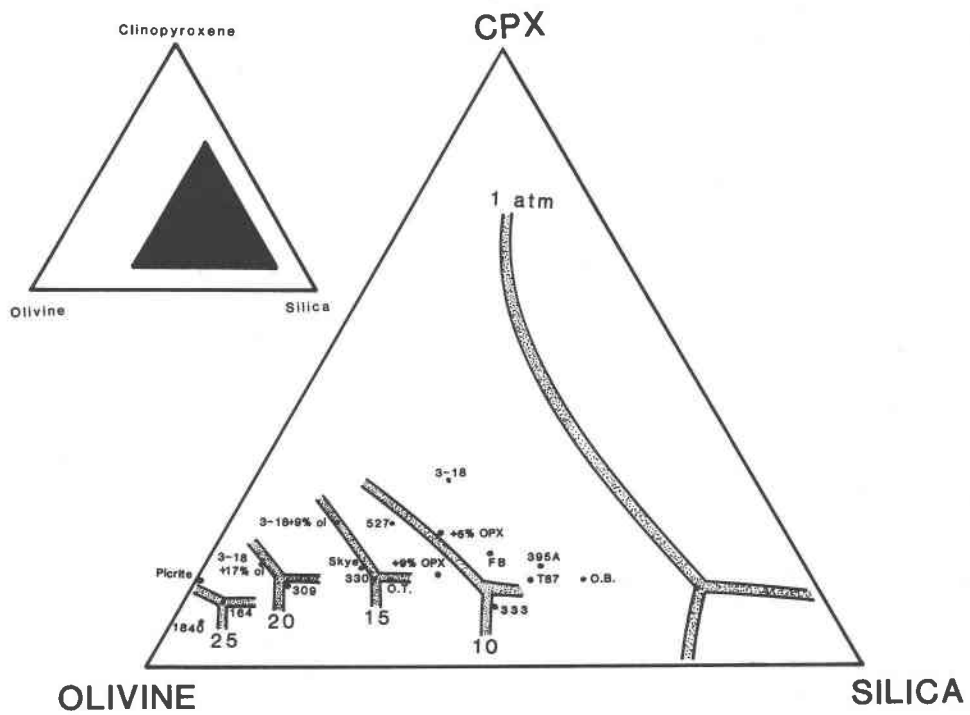

Fig. 3. Pseudo-liquidus phase diagram projected from anorthite. See text for discussion. The apices of the triangle are: (top) $CPX_{60}OL_{10}SIL_{30}$ (left) $OL_{60}CPX_{10}SIL_{30}$ (right) $SIL_{80}CPX_{10}OL_{10}$. 1 atm phase equilibria are from Walker *et al.* (1979).

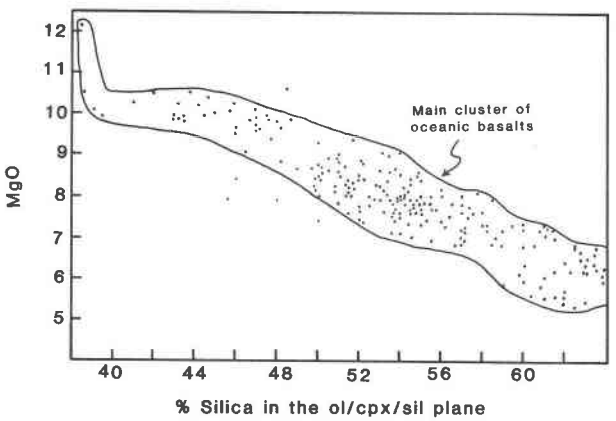

Fig. 4. MgO content of oceanic basalt glasses versus the percentage of normative silica in the olivine–clinopyroxene–silica plane. Sources of data are listed in the text. Note the decrease of MgO with increasing normative silica.

In order to avoid biasing the data to those locations that are heavily represented in the listing by Melson *et al.* (1977), only one sample per location is included on these plots and projections unless there was a significant variation in compositions at a site.

Melson *et al.*, 1977; Bryan and Moore, 1977; Wood *et al.*, 1979 and others) within the olivine–clinopyroxene–silica plane, shows that the most "primitive" oceanic basalts (*i.e.*, those basalts with >9.5% MgO) lie at the silica-poor end of the basalt cluster. The MgO content decreases and the normative silica content increases during differentiation. For this reason, it is critical to look at the silica-poor (least differentiated) end of the basalt cluster when evaluating the compositions of primary oceanic basalts.

The processes of melt production, magma ascent, crystallization differentiation, and magma mixing probably operate in a very complex manner to produce effects that are, at present, difficult to distinguish from each other in oceanic basalt petrogenesis. In order to evaluate the different models for the genesis of primary oceanic basalts, first consider melting of the mantle at ~10 kbar to produce primary oceanic basalts as suggested by Kushiro (1973), Fujii and Kushiro (1977), Presnall *et al.* (1979) and Fujii and Bougault (1983). The primary melt in equilibrium with OL + OPX + CPX + SP/PLAG at 10 kbar would project at or near the 10 kbar pseudo-invariant point shown in Figures 5 and 6.

A primary magma generated at 10 kbar and subsequent-

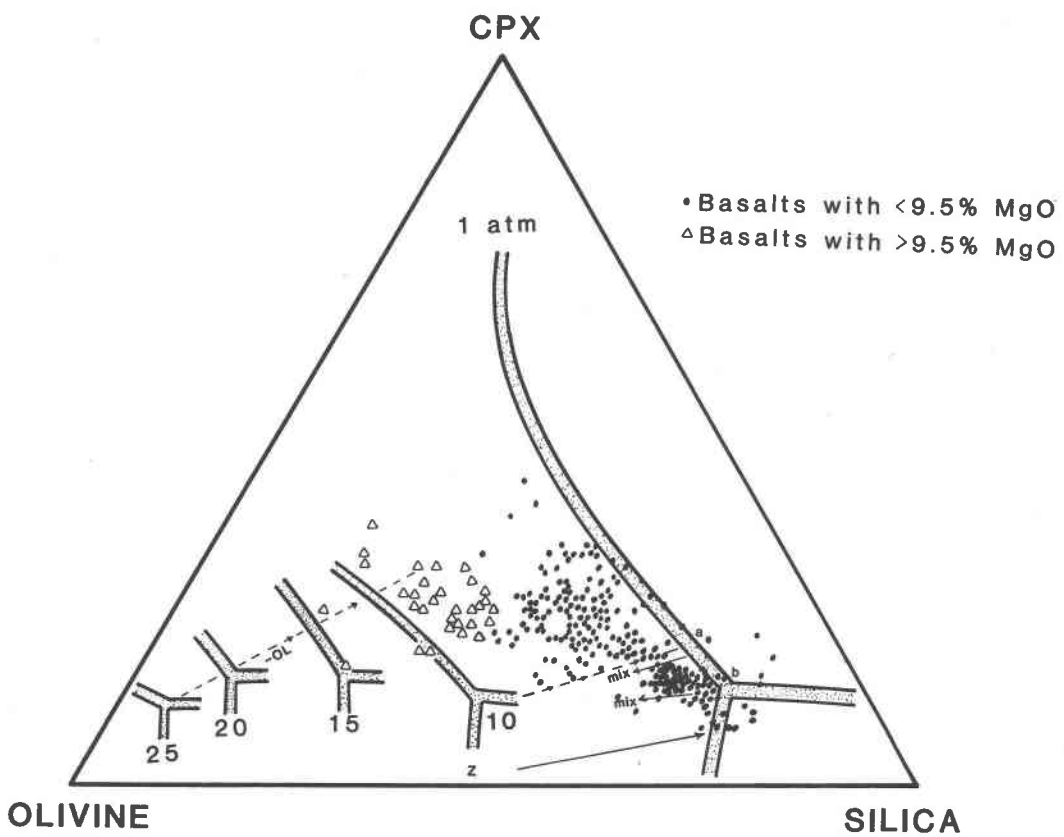

Fig. 5. Projection of oceanic basalt glasses from anorthite onto a part of the olivine–clinopyroxene–silica plane. Phase equilibria boundaries and triangle apices are from Fig. 3.

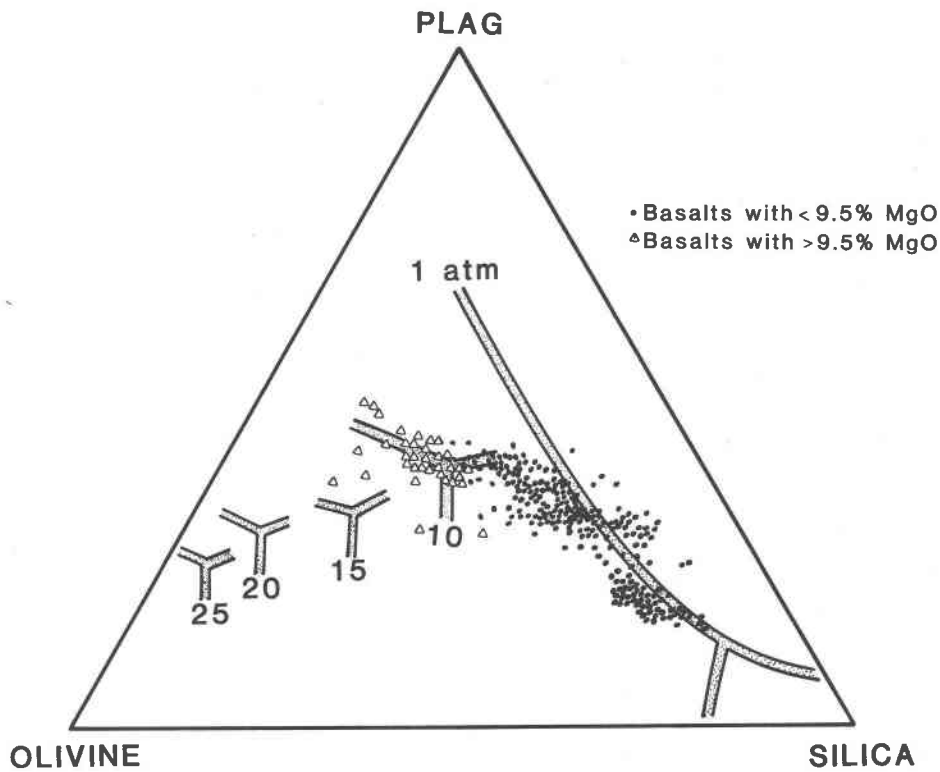

Fig. 6. Projection of oceanic basalt glasses from clinopyroxene onto the olivine–plagioclase–silica plane. Phase equilibria boundaries and triangle apices are from Fig. 2.

ly transported to a near-surface magma chamber will undergo olivine fractionation followed by olivine + plagioclase, olivine + plagioclase + clinopyroxene, and finally olivine + plagioclase + clinopyroxene + orthopyroxene as the liquid composition changes from the 10-kbar pseudoinvariant point to points a and b (Fig. 5) during crystallization. Even with open-system fractionation (O'Hara, 1977; Rhodes and Dungan, 1979) in which the crustal magma chamber is periodically refilled with an aliquot of primary magma, periodic injection of the primary magma generated at 10 kbar into the fractionating magma chamber (*a-b*) will produce mixed basaltic compositions that project to the silica-rich (right-hand) side of the olivine subtraction line drawn from the 10-kbar pseudo-invariant point (Fig. 5). Similarly, fractionation at high pressures within the mantle will produce basalts that lie further to the silica-rich side of this olivine subtraction line because combinations of the fractionating phases (OL, OPX, CPX, GAR, SP) lie to the silica-poor side of the pseudo-invariant point.

More advanced melting of the mantle at 10 kbar to leave a spinel harzburgite residuum rather than the spinel lherzolite residuum model discussed above would result in even higher normative silica in the derivative basalts than in the lherzolite residuum model. If melting of the mantle at 10 kbar proceeds until a spinel harzburgite residuum remains, producing a primary liquid such as "Z" (Fig. 5), the basalts derived from "Z" would crystallize orthopyroxene before clinopyroxene and would be unlike most oceanic basalts.

It is unlikely that melting at such low pressures (10 kbar or less) is a major process in the production of "primitive" oceanic basalts with >9.5% MgO because the vast majority of these basalts lie significantly to the silica poor (left-hand) side of the olivine subtraction line drawn from the 10 kbar pseudo-invariant point. If it is assumed that those basalts with <9.5% MgO are derived from the "primitive" basalts shown in Figs. 5 and 6 with >9.5% MgO by crystallization and mixing processes, then melting at ≤10 kbar is considered less preferable than models involving primary magma generation at higher pressures (15 to 25 kbar).

O'Hara (1968) has suggested that the primary magmas from which most oceanic basalts are ultimately derived are high-MgO basalts generated at 25 to 30 kbar. The experimental data on NT-23, which has olivine + orthopyroxene + clinopyroxene + garnet on the liquidus at 25 kbar, agrees with O'Hara's proposal. In fact, if the simplest model involving only olivine fractionation between genesis and eruption is considered, the majority of oceanic basalts with >9.5% MgO lie on or near the olivine subtraction line drawn from the 25 kbar pseudo-invariant

point. Open-system fractionation within the crust, in which pulses of a high-MgO basalt similar to the composition of the 25 kbar pseudo-invariant point glass are periodically injected into a magma chamber (O'Hara, 1977) will generate complex mixing-fractionation cycles similar to those shown in Fig. 5 that result in a spectrum of oceanic basalt compositions that cluster near the 1 atm olivine + plagioclase ± clinopyroxene cotectics. An additional process that needs to be considered, the high pressure fractionation of wehrlite or clinopyroxenite from primary oceanic basalts (Bender *et al.*, 1978; Bence *et al.*, 1979; Elthon *et al.*, 1982), will also result in increasing normative silica in the derivative basalts, driving the compositions of basalts towards the right-hand (silica-rich) side of the basalt cluster. Thus, magma mixing or crystal fractionation processes will clearly have the tendency to produce evolved basalts whose compositions are displaced toward normative silica enrichment relative to the primary basalt from which they are derived. In examining the petrogenesis of a suite of cogenetic oceanic basalts derived from a primary liquid by these processes, those basalts that lie at the left-hand (silica-poor) end of a given suite would be the most indicative of the conditions of origin of the primary magma. We interpret the observation that most of the "primitive" oceanic basalts with >9.5% MgO are close to olivine-controlled liquid lines of descent from the 15 to 25 kbar isobaric pseudo-invariant points to indicate that those basalts have been derived from primary magmas generated within this pressure interval.

Other types of evidence from oceanic rocks may indicate that the final pressure of equilibration for some primary oceanic basalts with the upper mantle may be at >20 kbar pressure. Hamlyn and Bonatti (1980) describe equant pyroxene + spinel clusters in the Owen F. Z. ultramafics that, because of the high proportion of spinel to pyroxene, they attributed to the breakdown of garnet via the reaction: olivine + garnet ⇄ pyroxene + spinel. The presence of garnet in these peridotites would imply a pressure of ≳25 kbar. Further evidence on the equilibration of some of the Owen F. Z. ultramafics with a primary magma at high pressures is indicated by the comparatively high abundances of Al_2O_3 in orthopyroxenes from the harzburgites. Elthon (1981) determined the melting relationships of two oceanic peridotites, one from the Owen F. Z. and the other from the Atlantic Ocean, at high pressure and found that the Al_2O_3 content of both orthopyroxenes and clinopyroxenes decreases with increasing degree of melting at 10 and 20 kbar. At any percentage of melting, the aluminum content of both clinopyroxene and orthopyroxene increases with increasing pressure. Orthopyroxenes in the Owen F. Z. harzburgite contain 4.8–5.2% Al_2O_3. The data of Elthon (1981 and in prep.) and Jaques and Green (1980) indicate that at ≤20 kbar, ≲3.5% Al_2O_3 is found in harzburgite orthopyroxenes, compared to the 5.0±0.2% Al_2O_3 in the Owens F. Z. harzburgite orthopyroxenes. Because these harzburgites contain 50 to 100 times as much orthopyroxene as spinel, it is unlikely that the Al_2O_3 contents of the harzburgite orthopyroxenes have been significantly changed due to subsolidus equilibration with the spinels, even though the spinels may have changed significantly. These features suggest that the final equilibration of a melt with these orthopyroxenes was at pressures greater than 20 kbar.

The olivine composition in equilibrium with the pseudo-invariant point liquid at 25 kbar (run 164) is $Fo_{89.5}$ which falls within the range ($Fo_{89.0–90.4}$) reported from the Owen Fracture Zone ultramafics (Hamlyn and Bonatti, 1980). This agreement between the liquidus olivine compositions in our experiments at 25 kbar and the olivine compositions in the Owen F. Z. ultramafics, when coupled with the Al_2O_3 contents of orthopyroxenes in harzburgites, supports our inferences based on the projection of oceanic basalts onto high-pressure pseudo-liquidus phase diagrams that many of the "primitive" oceanic basalts are ultimately derived from primary high-MgO basalts generated at pressures >15 kbar.

Concluding remarks

The model described above, in which primary oceanic basalts are generated by partial melting at 15 to 25 kbar, is in agreement with previous models by O'Hara (1968), Green *et al.* (1979), and Stolper (1980), who propose that most oceanic basalts are derived from primary magmas that are generated at 15 to 30 kbar pressure. These previous pressure estimates are derived, for the most part, by assuming that simple olivine fractionation has been the process that has occurred between melting and eruption. If it is assumed that only olivine fractionation occurs between melting and eruption, olivine addition lines drawn from primitive oceanic basalts (>9.5% MgO) in an effort to reconstruct the composition of the primary magma prior to olivine fractionation result in intersections with the isobaric pseudoinvariant points at 15 to 25 kbar (see Figs. 5 and 6). This indicates the general agreement between the models of O'Hara, Green *et al.*, Stolper, and Elthon and Scarfe, in which primary oceanic basalts are generated between 15 and 25 kbar.

We consider it likely that the evolutionary processes involved in oceanic basalt genesis are considerably more complex than these simple olivine fractionation models may imply. For example, evidence on the role of high-pressure crystal fractionation in the evolution of oceanic basalts is obtained from Elthon *et al.* (1982) who interpret the basal ultramafic cumulates from the North Arm Mountain massif of the Bay of Islands to have formed by high-pressure crystallization. On the basis of other ophiolite massifs that have similar cumulate ultramafic mineral assemblages and mineral compositions, as well as data from oceanic basalts, Elthon *et al.* propose that high-pressure crystal fractionation may be a common process in the evolution of oceanic basalts.

Mineral assemblages within the ultramafic cumulates of North Arm Mountain indicate that basaltic liquids have a

strong tendency to fractionate to lower pressure isobaric pseudoinvariant points during magma ascent (Elthon *et al.*, 1982). As an example, a primary magma generated in equilibrium with a harzburgite residuum at 20 kbar that subsequently undergoes high-pressure crystallization (dunite → wehrlite → lherzolite) at 10 kbar until the liquid is in equilibrium with OL + OPX + CPX + SP would project at the 10 kbar pseudo-invariant point and might appear (erroneously) to represent a primary magma generated at 10 kbar. If high-pressure fractionation of this type occurs within the sub-oceanic mantle, estimates of the pressure of melting in the mantle based on pseudo-liquidus phase diagrams must represent minimum pressures. It is possible that the oceanic basalts studied experimentally by Kushiro (1973) and Fujii and Kushiro (1977), which crystallize a comparatively Fe-rich plagioclase lherzolite assemblage at 7.5 to 8 kbar, have experienced a similar high-pressure crystallization history in which the liquid has been modified to the 7.5 to 8 kbar pseudo-invariant point.

It is also interesting to note that most "primitive" oceanic basalts (>9.5% MgO) lie along or adjacent to the 10 kbar OL + CPX + SP + LIQ isobaric pseudounivariant curve (see Figs. 5 and 6). One possible cause of this alignment of "primitive" oceanic basalts along the isobaric pseudo-univariant curve is that these basalts may have undergone crystal fractionation at high pressures, with those basalts that project closest to the isobaric pseudo-invariant point having undergone the greatest degree of crystal fractionation.

On the basis of the above discussion, we believe that oceanic basalts may commonly undergo high-pressure crystallization prior to eruption. As briefly noted above, the effect of high-pressure crystal fractionation on these pseudo-liquidus phase diagrams is to drive residual liquids towards silica enrichment, *i.e.*, towards the right on Figures 5 and 6. Because of the difficulty in quantitatively evaluating the magnitude of the effect that high-pressure fractionation has had on individual "primitive" oceanic basalts, the extent of enrichment in normative silica as a consequence of this process is uncertain.

In evaluating overall scenarios for the petrogenesis of oceanic basalts, it is considered likely that a combination of high pressure fractionation and/or magma mixing processes may be important, even in those primitive basalts with >9.5% MgO. Recognizing that both of these processes tend to produce an increase in normative silica within the melt, we prefer a model for the origin of primary oceanic basalts at 15 to 25 kbar. In this model, these primary magmas are modified by a combination of high-pressure crystal fractionation and magma mixing to produce the more abundant oceanic basalts with 7.5 to 9.5% MgO.

The discussion above has been based on the assumption that the majority of oceanic basalts with <9.5% MgO are differentiates of the "primitive" basalts with >9.5% MgO, which are shown in Figures 5 and 6. It should be noted that for many of these basalts, which have equilibrated to the low-pressure cotectics, this lineage is not readily constrained. In fact, it is possible that basalts that project to the center of the group with <9.5% MgO are derived by the crystallization of a primary magma that, by virtue of having been produced at 5 to 10 kbar was chemically different from those basalts with >9.5% MgO shown in Figures 5 and 6. Until the processes of crystallization and magma mixing are more adequately quantified, it will not be possible to unambiguously ascertain the pressure of origin for the primary magmas related to many of the evolved oceanic basalts with <9.5% MgO. For this reason, we do not propose a lower-most pressure limitation for the production of primary oceanic basalts. Rather, we suggest that if primary oceanic basalts are produced at ≤10 kbar, these basalts would not be like most of those basalts with >9.5% MgO that are recovered from the present-day oceanic basins.

Acknowledgments

The experimental work was performed at the Geophysical Laboratory of the Carnegie Institution of Washington while the authors were a predoctoral fellow (DE) and guest investigator (CMS). Dr. H. S. Yoder Jr. is thanked for his continued interest and for giving us the opportunity to work at the Geophysical Laboratory. The Carnegie Institution of Washington is thanked for financial support.

Most of the microprobe analyses and follow-up studies were performed while Elthon was a Research Associate at the Smithsonian Institution in Washington, D. C., and Scarfe had returned to the University of Alberta. W. G. Melson, E. Jarosewich, and J. Nelen are thanked for their assistance with the analytical aspects of this project and for discussions concerning the results.

Scarfe acknowledges support from Canadian NSERC grant A8394. Elthon acknowledges support from the United States National Science Foundation through grants EAR80-26445 and OCE 81-21232. Drs. T. Fujii, D. Walker, and an anonymous reviewer are thanked for their critical reviews.

References

Albee, A. L. and Ray, L. (1970) Correction factors for electron microprobe microanalysis of silicates, oxides, carbonates, phosphates, and sulfates. Analytical Chemistry, 42, 1408–1414.

Bence, A. E. and Albee, A. (1968) Empirical correction factors for the electron microanalysis of silicates and oxides. Journal of Geology, 76, 382–401.

Bence, A. E., Baylis, D. M., Bender, J. F. and Grove, T. L. (1979) Controls on the major and minor element chemistry of midocean ridge basalts and glasses. In M. Talwani, C. G. Harrison and D. E. Hayes, Eds., Deep Drilling Results in the Atlantic Ocean: Oceanic Crust, p. 331–341. American Geophysical Union, Washington, D. C.

Bender, J. F., Hodges, F. N. and Bence, A. E. (1978) Petrogenesis of basalts from the project FAMOUS area: Experimental study from 0 to 15 kbars. Earth and Planetary Science Letters, 41, 277–302.

Bonatti, E. and Hamlyn, P. R. (1978) Mantle uplifted block in the Western Indian Ocean. Science, 201, 249–251.

Bonatti, E. and Hamlyn, P. R. (1981) Oceanic ultramafic rocks.

In C. Emiliani, Ed., The Sea, vol. 7, p. 241–283. Wiley, New York.

Bonatti, E., Honnorez, J. and Ferrara, G. (1970) Equatorial Mid-Atlantic Ridge: Petrologic and Sr-isotopic evidence for an alpine-type rock assemblage. Earth and Planetary Science Letters, 9, 247–256.

Boudier, F. and Coleman, R. G. (1981) Cross section through the peridotite in the Samail Ophiolite, southeastern Oman Mountains. Journal of Geophysical Research, 86, 2573–2592.

Boyd, F. R. and England, J. L. (1960) Apparatus for phase equilibrium measurements at pressures up to 50 kilobars and temperatures up to 1750°C. Journal of Geophysical Research, 65, 741–748.

Bryan, W. B., Finger, L. W. and Chayes, F. (1969) Estimating proportions in petrographic mixing equations by least-squares approximation. Science, 163, 926–927.

Bryan, W. B. and Moore, J. G. (1977) Compositional variation of young basalts in the Mid-Atlantic Ridge Rift valley near 36°49′ N. Geological Society of America Bulletin, 88, 556–570.

Casey, J. F., Dewey, J. F., Fox, P. J., Karson, J. A. and Rosencrantz, E. (1981) Heterogeneous nature of oceanic crust and upper mantle: A perspective from the Bay of Islands ophiolite complex. In C. Emiliani, Ed., The Sea, vol. 7, p. 305–338. Wiley, New York.

Clarke, D. B. (1970) Tertiary basalts of Baffin Bay: possible primary magma from the mantle. Contributions to Mineralogy and Petrology, 25, 203–224.

Davies, H. L. (1971) Peridotite–gabbro–basalt complex in Eastern Papua: An overthrust plate of oceanic mantle and crust. Australian Bureau of Mines Resources Bulletin, 128, 1–48.

Delaney, J. R., Muenow, D. W. and Graham, D. G. (1978) Abundance and distribution of water, carbon, and sulfur in the glassy rims of submarine pillow lavas. Geochimica et Cosmochimica Acta, 42, 581–594.

Dmitriev, L. V. (1969) Origin of the ultrabasic rocks in the rift zones of the Indian Ocean Ridge. Geochemistry International, 6, 923–931.

Echeverria, L. M. (1980) Tertiary or Mesozoic komatiites from Gorgona Island, Columbia: field relations and geochemistry. Contributions to Mineralogy and Petrology, 73, 253–266.

Engel, C. G. and Fisher, R. L. (1975) Granitic to ultramafic rock complexes of the Indian Ocean ridge system, Western Indian Ocean. Geological Society of America Bulletin, 86, 1553–1578.

Elthon, D. (1979) High magnesia liquids as the parental magma for ocean floor basalts. Nature, 278, 514–518.

Elthon, D. (1980) The Petrology of the Tortuga Ophiolite Complex, Southern Chile: Implications for igneous and metamorphic processes at oceanic spreading centers. Ph. D. thesis, Columbia University, New York.

Elthon, D. (1981) Melting relationships of two oceanic peridotites at high pressures. Abstracts volume for AGU Chapman Conference on the Generation of the Oceanic Lithosphere.

Elthon, D. (1983) Isomolar and Isostructural pseudo-liquidus phase diagrams for oceanic basalts. American Mineralogist, 68, 506–511.

Elthon, D., Casey, J. and Komor, S. (1982) Mineral chemistry of ultramafic cumulates from the North Arm Mountain massif of the Bay of Islands ophiolite: Evidence for high-pressure crystal fractionation of oceanic basalts. Journal of Geophysical Research, 87, 8717–8734.

Elthon, D. and Scarfe, C. M. (1980) High-pressure phase equilibria of a high-magnesia basalt: Implications for the origin of mid-ocean ridge basalts. Carnegie Institution of Washington Yearbook, 79, 277–281.

Francis, D. M. and Hynes, A. J. (1979) Komatiite-derived tholeiites in the proterozoic of New Quebec. Earth and Planetary Science Letters, 44, 473–481.

Fujii, T. and Bougault, H (1983) Melting Relations of a magnesian abyssal tholeiite and the origin of MORBs. Earth and Planetary Science Letters, 62, 283–295.

Fujii, T. and Kushiro, I. (1977) Melting relations and viscosity of an abyssal tholeiite. Carnegie Institution of Washington Yearbook, 76, 461–465.

Green, D. H., Hibberson, W. D. and Jacques, A. L. (1979) Petrogenesis of mid-ocean ridge basalts. In M. W. McElhinney, Ed., The Earth: Its origin, structure, and evolution, p. 265–299. Academic Press, London.

Green, D. H. and Ringwood, A. E. (1967) The genesis of basaltic magmas. Contributions to Mineralogy and Petrology, 15, 103–190.

Hadidiacos, C. (1972) Temperature controller for high-pressure apparatus. Carnegie Institution of Washington Yearbook, 71, 620–622.

Hamlyn, P. R. and Bonatti, E. (1980) Petrology of mantle-derived ultramafics from the Owen Fracture Zone, northwest Indian Ocean: Implications for the nature of the oceanic upper mantle. Earth and Planetary Science Letters, 48, 65–79.

Harrison, W. J. (1981) Partitioning of REE between minerals and coexisting melts during partial melting of a garnet lherzolite. American Mineralogist, 66, 242–259.

Hoover, J. D. and Presnall, D. C. (1981) Partial melting of simplified lherzolite in the system CaO–MgO–Al_2O_3–SiO_2–Na_2O from 1 ATM to 20 kb. Abstract volume of the AGU Chapman Conference on the Generation of the Oceanic Lithosphere.

Jackson, E. D., Green, H. W. and Moores, E. M. (1975) The Vourinos ophiolite, Greece: cyclic units of lineated cumulates overlying harzburgite tectonite. Geological Society of America Bulletin, 86, 390–398.

Jaques, A. L. and Green, D. H. (1980) Anhydrous melting of peridotite at 0–15 Kb pressure and the genesis of tholeiitic basalts. Contributions to Mineralogy and Petrology, 73, 278–310.

Karson, J. A., Elthon, D. and DeLong, S. E. (1983) Ultramafic intrusions in the Lewis Hills Massif, Bay of Islands ophiolite, Newfoundland: Implications for igneous processes at oceanic fracture zones. Geological Society of America Bulletin, 94, 15–29.

Kushiro, I. (1973) Origin of some magmas in oceanic and circumoceanic regions. Tectonophysics, 17, 211–222.

Melson, W. G. (1978) Chemical stratigraphy of Leg 45 basalts: Electron probe analyses of glasses. In Melson, W. G. Rabinowitz, P. D. *et al.*, Initial reports of the Deep Sea Drilling Project, v. 45, p. 507–512. U. S. Government Printing Office, Washington, D. C.

Melson, W. G., Byerly, G. R., Nelen, J. A., O'Hearn, T., Wright, T. L. and Vallier, T. (1977) A catalog of the major element chemistry of abyssal volcanic glasses. Mineral Sciences Investigations: Smithsonian Contributions to the Earth Sciences, 19, 31–60.

Melson, W. G. and Thompson, G. (1971) Petrology of a transform fault zone and adjacent ridge segments. Philosophical Transactions of the Royal Society of London, A268, 423–441.

Moore, J. G. (1970) Water content of basalt erupted on the ocean

floor. Contributions to Mineralogy and Petrology, 28, 272–279.
Mysen, B. O. and Kushiro, I. (1977) Compositional variations of coexisting phases with degree of melting of peridotite in the upper mantle. American Mineralogist, 62, 843–865.
O'Hara, M. J. (1968) The bearing of phase equilibria studies on the origin and evolution of basic and ultrabasic rocks. Earth Science Reviews, 4, 69–133.
O'Hara, M. J. (1977) Geochemical evolution during fractional crystallization of a periodically refilled magma chamber. Nature, 266, 503–507.
Presnall, D. C., Dixon, J. R., O'Donnell, T. H. and Dixon, S. A. (1979) Generation of mid-ocean ridge tholeiites. Journal of Petrology, 20, 3–35.
Rhodes, J. M. and Dungan, M. A. (1979) The evolution of ocean-floor basaltic magmas. In M. Talwani, C. G. Harrison and D. E. Hayes, Eds., Deep Drilling Results in the Atlantic Ocean: Oceanic Crust, p. 262–272. American Geophysical Union, Washington, D.C.
Scarfe, C. M., Mysen, B. O. and Rai, C. S. (1979) Invariant melting behavior of mantle material: Partial melting of two lherzolite nodules. Carnegie Institution of Washington Yearbook, 78, 498–501.
Stolper, E. (1980) A phase diagram for mid-ocean ridge basalts: Preliminary results and implications for petrogenesis. Contributions to Mineralogy and Petrology, 74, 13–27.
Thompson, R. N. (1974) Primary basalts and magma genesis. I. Skye, northwest Scotland. Contributions to Mineralogy and Petrology, 45, 317–341.
Tilley, C. E. and Yoder, H. S., Jr. (1964) Pyroxene fractionation in mafic magma at high pressures and its bearing on basalt genesis. Carnegie Institution of Washington Yearbook, 63, 114–121.
Upadhyay, H. D. (1978) Phanerozoic peridotitic and pyroxenitic komatiites from Newfoundland. Science, 202, 1192–1195.
Walker, D., Shibata, T. and DeLong, S. E. (1979). Abyssal tholeiites from the Oceanographer Fracture Zone. II. Phase equilibria and mixing. Contributions to Mineralogy and Petrology, 70, 111–126.
Wilson, R. A. M. (1959) The geology of the Xeros-Trodoos Area. Geological Survey Department of Cyprus, Memoir 1, 1–184.
Wood, D. A., Tarney, J., Varet, J., Saunders, A. D., Bougault, H., Joron, J. L., Treuil, M., and Cann, J. R. (1979) Geochemistry of basalts drilled in the North Atlantic by IPOD leg 49: Implications for mantle heterogeneity. Earth and Planetary Science Letters, 42, 77–97.

Manuscript received, December 23, 1981;
accepted for publication, July 5, 1983.